DOI: 10.5604/01.3001.0013.7937

Volume 96 • Issue 2 • October 2019

Journal of Achievements in Materials and Manufacturing Engineering

International Scientific Journal published monthly by the World Academy of Materials and Manufacturing Engineering

# Measurements and numerical simulations of laser hardening and remelting thermal cycles

**T. Kik *, B. Wyględacz**

Department of Welding Engineering, Silesian University of Technology, ul. Konarskiego 18a, 44-100 Gliwice, Poland

* Corresponding e-mail address: tomasz.kik@polsl.pl

## ABSTRACT

**Purpose:** of these researches was to investigate the influence of thermal cycles recording conditions and comparing them with the calculated by FEM. This approach allows proposing a new way of determining the technological conditions of the process, based on numerical analyses.

**Design/methodology/approach:** Thermal cycles of high power diode laser hardening and remelting was recorded and calculated by FEM. Results of metallographic examinations were compared with numerical simulations results, as well as the thermographic pictures. Acquisition errors during the thermal cycles were also defined.

**Findings:** Due to the fact that the it was used FEM, comparison of the numerical analyses with real test results was performed for laser hardening and remelting process.

**Research limitations/implications:** For complete information it is needed to collect bigger database of the results and prepare also hardness calculation model for WCL steel.

**Practical implications:** The result of the presented work is to signal a methodology that allows obtaining information on the impact of the parameters of the laser hardening and remelting process on the properties of the treated samples. Not without significance is the fact that the use of FEM eliminates in this case a lot of errors that in real tests can distort the result.

**Originality/value:** The researches were provided for high power diode laser hardening and remelting. The influence of heat input on layers properties and theirs structure was defined. Results were compared with thermographic pictures and calculated cases.

**Keywords:** Hardening, Remelting, WCL steel, Diode laser, Thermal cycle, SYSWELD, Numerical simulation

**Reference to this paper should be given in the following way:**

T. Kik, B. Wyględacz, Measurements and numerical simulations of laser hardening and remelting thermal cycles, Journal of Achievements in Materials and Manufacturing Engineering 96/2 (2019) 69-82.

## ANALYSIS AND MODELLING

## 1. Introduction

High-power industrial lasers have long ceased to be new on the market. Their common use results from many advantages of the laser beam, i.e. precise control of the method and amount of heat input, contactless heat transfer to the material being processed or high process efficiency [1-4]. Among many welding techniques, surface treatment technologies using a laser beam are an interesting part. The possibility of focusing the laser beam and the accuracy of the device power control allows for precise heating of selected areas of the processed surface. As a technological process, laser hardening is a process of changing the surface properties of iron-based metal alloys, with the aim of increasing abrasion resistance. Surface hardening is used in the production of tools, cams, gears, shafts, automotive industry, in the production of turbines and in many other industries [5-11]. Hardened layers are first and foremost required for hardness as well as for resistance to dynamic loads. The use of laser techniques has a number of advantages over volume hardening. First of all, it avoids excessive hardening deformations and significantly reduces the risk of potential cracks related to them. Very high heating and cooling speeds result in the existence of a fine-grained structure with high hardness, and at the same time sufficient resistance to dynamic loads, allowing the use of laser-hardened layers without annealing, making this process much more efficient and economically profitable. The hardness obtained in laser hardened layers are usually higher than in conventionally hardened layers, which means that after tempering, these layers have better properties than when using conventional hardening methods [2-12]. The thickness of the laser hardened layer is usually from 0.25 mm to 0.75 mm [7]. The same can be said about the remelting and laser alloying processes used to change the properties of the surface layer. However, laser surface treatment processes also have specific requirements. There is a need to maintain an adequate residence time at austenitizing temperatures to dissolve all carbon and alloying elements in the matrix, while not allowing the material to melt in the case of quenching, to provide rapid cooling and low cooling end temperatures using one thermal cycle controlled by a number of laser beam parameters and its trajectory [3-8,13].

The use of numerical methods to precisely define and even design the heat cycle of the hardening and laser remelting process allows the introduction of a new quality in heat treatment processes. Properly conducted numerical analyzes give the possibility of predicting changes in temperature fields during the process, which allows determining the volume distribution of thermal cycles of hardening, and as a result optimizing the depth, shape, and properties of the hardened layer [14,15]. The tools for conducting numerical analyses can support not only the preparation of technology but also laboratory tests [8,10,11].

Most widespread method of high temperature and high variability thermal cycle recording is the use of the thermoelectric effect. To gather the most valuable data often surface measurements are not sufficient. To perform thermal cycle measurement from quasi-inside of the material typically small hole is drilled and thermocouple is placed on the bottom of said hole and secured in place by condenser welding. The physical measurement to digital data result path enables us to divide errors during acquisition into two main categories:

- physical measurement – there are mostly connected to the faulty placement or fabrication of thermocouples, to small contact patch between spherical thermocouple and metal surface, changes in sample properties caused by drilled hole,
- acquisition errors – there are wildly known and caused by discretization in time and value, and non-ideal characteristic of digital measurement circuits and discrepancy between thermocouple and modelled temperature-voltage characteristic. Based on the prior work of authors much more impacting and much harder to eliminate are errors of the first group [9,14-17].

## 2. Welding numerical simulations

On the present market, there is a lot of software solution, which are more or less suitable for numerical simulations of welding processes. In the presented works SYSWELD – the product of ESI Group was used. SYSWELD covers now the complete area of non-linear Finite Element Method (FEM) analyses such as non-linear heat conduction, non-linear geometry of large distortions, isotropic and kinematic material hardening or metallurgical transformations. The connection of many different phenomena present during the welding process results in very high precision of simulations results and their coherence with real welding results. It is possible to simulate welding with or without filler material using heat sources with physical contact (friction stir welding, resistance welding) and without contact (electric arc, laser and electron beam). Similarly wide is a range of possible analyses of heat treatment. It is possible to analyse for example tempering, hardening, carburizing, nitriding. Input data for calculations are the same as data in the Welding

Procedure Specification prepared and also based on the typical knowledge and experience of welding engineers and moderate from the FEM area. Important is fact, that results of these analyses are not only the temperature distribution fields but also metallurgical phases, distortions, stresses and hardness distribution [14,15,18-21].

To ensure a high level of results accuracy and real results compatibility, very important are well-prepared material databases. In SYSWELD mechanical properties are defined as dependant on the temperature and metallurgical phases mixture. Outside of the thermo-mechanical data such as heat transfer coefficient, specific heat/enthalpy, density, Young modulus, Poisson's ratio, Yield strength or strengthening important are also metallurgical properties. SYSWELD takes into consideration metallurgical phase changes, austenite transformation kinetic during heating (TTA diagram) and ferrite, bainite and martensite transformation during cooling (CCT, TTT diagrams) [15,18,22-24].

Except the well-prepared material database, also very important is a proper definition of the heat source model. From the FEM analysis point of view, a heat source is modelled in SYSWELD by a volume density of energy applied to elements Q(x,y,z), which move along the welding trajectory. All process parameters are included in the definition of heat source: energy, efficiency coefficient, torch shape, etc. FORTRAN type function used for description heat source depends on the current location and time. It consists on the mathematical description of the energy distribution and the welding trajectory [19,22-24].

"Volumetric density of energy" defined by this FORTRAN function on the current point depends on the distribution of density around the centre of the source and trajectory. In SYWELD except our own heat source definition, we have three predefined source shapes: 2D Gauss, double ellipsoid (also called Goldak's heat source) and 3D cone [18,19].

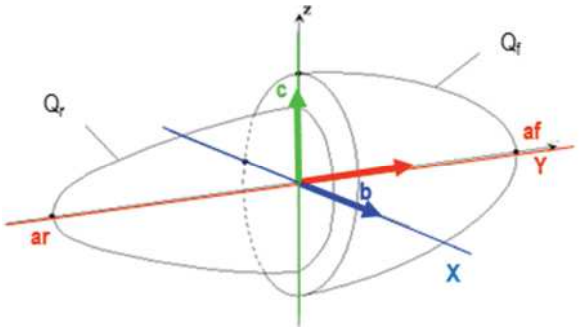


Fig. 1. Definition of a double ellipsoid heat source model in SYSWELD [18,19]

A volume heat source defined by a double ellipsoid is advised to simulate welding processes as a MIG and TIG. But thanks to the thermal load area shaping it is also possible to model other methods. As a standard, this model consists of two different single ellipsoids. Both ellipsoids are described by geometrical parameters as $a_f$, $a_r$, a, b and c as it was shown at Figure 1. By changing these parameters we have the advantages in the greater flexibility in the modelling of a heat source shape. SYSWELD enable the capability to introduce density energy $Q_R$ [W.mm$^{-3}$] which is divided on $O_f$ and $Q_r$ values. First of them is a heat energy density in the front half of the ellipsoid (maximum source frontal intensity) and second is the rear part (maximum source rear intensity), Figure 1. Values of the power density energy function $Q_R(x,y,z,t)$ is described by equations [18,19]:

for the front half of the heat source model

$$Q_R = Q_f \cdot e^{-\frac{x^2}{a_f^2}} \cdot e^{-\frac{y^2}{b^2}} \cdot e^{-\frac{z^2}{c^2}} \quad (1)$$

and for the rear half of the heat source model

$$Q_R = Q_r \cdot e^{-\frac{x^2}{a_r^2}} \cdot e^{-\frac{y^2}{b^2}} \cdot e^{-\frac{z^2}{c^2}} \quad (2)$$

Finally, the total power of this source model is:

$$P = \int_{structure} Q_R \quad (3)$$

## 3. Real laser hardening and remelting experiments

Preliminary tests were carried out on S355 steel samples to calibrate the model and to pre-establish thermal cycle recording conditions as well as thermographic images and measurement errors. Three beam power levels were used 1200 W, 1600 W and 2000 W. Welding speed was 0.5 m/min. The main tests were carried out on round samples of tool steel WCL 1.2343 with a diameter of 65 mm and a thickness of 10 mm supplied in the softened state, Table 1. ROFIN DL020 high power diode laser with a maximum beam power of 2000 W and dimensions of the laser beam spot 1.8x6.8 mm (at 82 mm focal length) was used in the laser hardening and remelting tests. Shielding gas was argon with a flow rate of 15 l.min$^{-1}$. The surface of the samples was ground and holes were made from below in which thermocouples were attached. K-type thermocouples have been welded at a distance of 3, 2, 1

and 0.5 mm from the surface to be treated at 10 mm intervals along the hardening/remelting line and then connected via compensating cables with Agilent 34970A recorder. The sampling rate with all 7 channels active was 5.8 Hz, and with one channel active sampling rate was 55 Hz. The lower sampling rate was sufficient to omit any loss of information. The FLIR a655sc thermal imaging camera was also mounted on the test stand, Figure 2. Thermovision examinations were carried out using a 25°x19° lens with a resolution of 640 by 480 points in the range of 100-2000°C. After the initial calibration of the test stand, a series of 10 tests of laser hardening with the parameters contained in Table 2 and 8 remelting beads with the parameters contained in Table 3 were performed. The samples were then subjected to metallographic examination to reveal the macrostructure of the beads.

To perform the simulation, a three-dimensional model was built consisting of 62477 nodes and 28926 solid elements. The model also selected nodes corresponding to the location of thermocouples at a distance of 3, 2, 1 and 0.5 mm from the machined surface at intervals of 10 mm, along the hardening/remelting line, Figures 2, 3.

Table 1.
Chemical composition of WCL steel according to PN-86 H-85021 standard, %wt.

| C | Mn | Si | P | S | Cr | Mo | V |
|---|---|---|---|---|---|---|---|
| 0.32-0.42 | 0.2-0.5 | 0.8-1.2 | max 0.030 | max 0.030 | 4.5-5.5 | 1.2-1.5 | 0.3-0.5 |

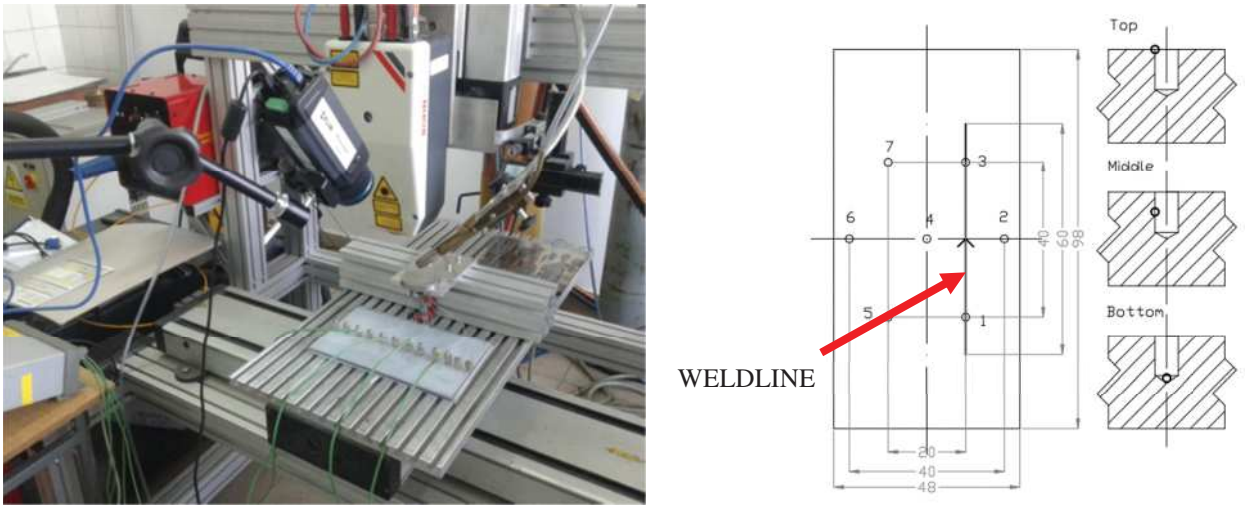


Fig. 2. View of the experimental stand (on the left) and thermocouple placement on samples and 3 types of thermocouple welding to circular channel (on the right)

Table 2.
Parameters of WCL steel surface hardening with ROFIN DL 020 laser

| Bead designation | H1 | H2 | H3 | H4 | H5 | H6 | H7 | H8 | H9 | H10 |
|---|---|---|---|---|---|---|---|---|---|---|
| Laser beam power, W | 400 | 600 | 700 | 800 | | 900 | 1000 | | 1100 | 1200 |
| Beam travelling speed, $m.min^{-1}$ | 0.2 | | 0.6 | | | 0.8 | | | 1.0 | |
| Energy per unit length, $J.cm^{-1}$ | 1200 | 600 | 700 | 800 | 600 | 675 | 750 | 600 | 660 | 720 |
| Remarks: focal length of the laser beam – 82 mm, dimensions of the laser beam spot – 1.8×6.8 mm, shielding gas – argon, flow rate – 15 $l.min^{-1}$ | | | | | | | | | | |

Table 3.
Parameters of WCL steel surface remelting with ROFIN DL 020 laser

| Bead designation | R1 | R2 | R3 | R4 | R5 | R6 | R7 | R8 |
|---|---|---|---|---|---|---|---|---|
| Laser beam power, W | 1000 | 1250 | 1500 | | | 1250 | | |
| Beam travelling speed, m.min$^{-1}$ | | 0.2 | | 0.15 | 0.1 | 0.3 | 0.4 | 0.5 |
| Energy per unit length, J.cm$^{-1}$ | 3000 | 3750 | 4500 | 5000 | 7500 | 2500 | 1875 | 1500 |
| Remarks: focal length of the laser beam – 82 mm, dimensions of the laser beam spot – 1.8×6.8 mm, shielding gas – argon, flow rate – 15 l.min$^{-1}$ | | | | | | | | |

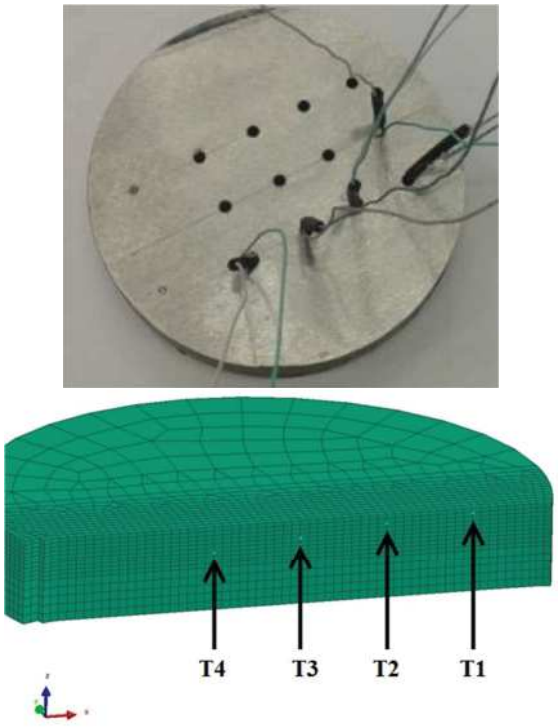


Fig. 3. View of the bottom of the sample with thermocouples and numerical model cross-section with the location of nodes corresponding to the mounted thermocouples

Due to the specific of High Power Diode Lasers (HPDL), which have mainly rectangular or square beam spot shape, it is not possible to use a 3D cone model as usually for lasers welding. Combination of available heat source models with the definition of volume where the heat source model affects the 3D model enables us the definition of the authorial method of imposing heat into the simulated model, which is very similar to the rectangular beam spot of HDPL lasers, Figure 4.

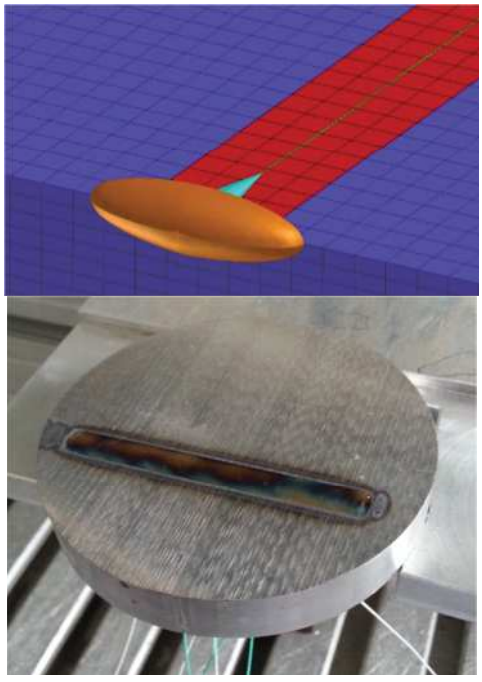

Fig. 4. View of heat source model – heat application area combination for HDPL heat source (red elements means the area where the only heat is applied form the Goldak's heat source model) and real remelted bead

Based on the calculations made and comparison of the temperature distribution on the cross-section with the corresponding macroscopic images, it was possible to determine the dimensions of the beads obtained. The calculation results, apart from the temperature field distributions, also allowed to obtain thermal cycles for selected mesh nodes, corresponding to the distribution of thermocouples in the tested samples. In addition, the surface temperature distributions also obtained allowed them to be compared with images recorded with a thermal imaging camera.

## 4. Tests and numerical simulations results

Heat cycles from simulation solutions were extracted from points corresponding to ideal thermocouple placement. Numeric values were plotted and the timing of acquired data was adjusted to simplify data analysis. The sample plot of simulation results against data from correctly placed thermocouples from sample welded with HDPL power 1600 is shown in Figure 5. Simulated heat cycles show much higher maximal values as well as higher heating and cooling speeds. It is a general tendency across all datasets.

Acquired thermal cycles in case of different placement of thermocouple in drilled channels differ from simulation results from 8 to 25% depending on laser beam power and element placement combination. For thermocouple no. 3 (see Fig. 6) which is one of the closest to the welding path, resulting in the most distinctive heat cycle.

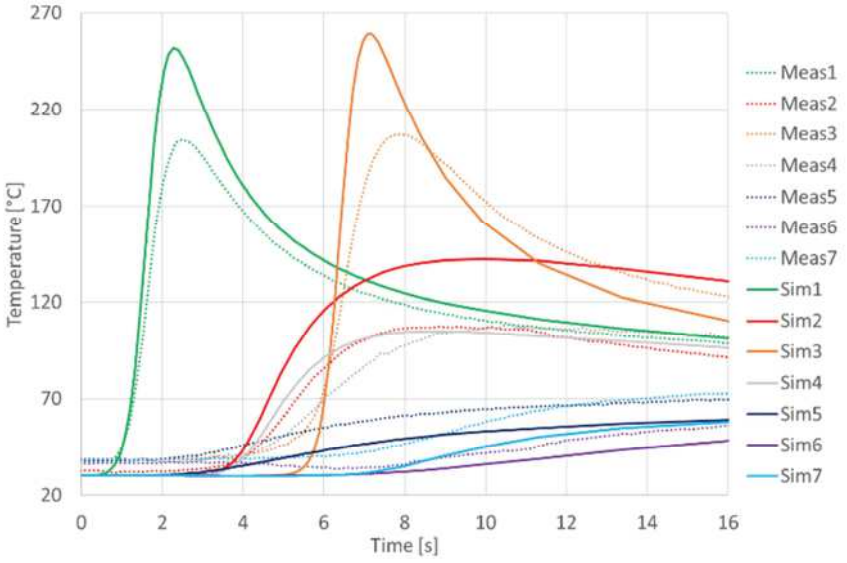


Fig. 5. Measured and simulated heat cycles. Data from Simulation and correctly placed thermocouples from sample welded with laser power of 1600 W

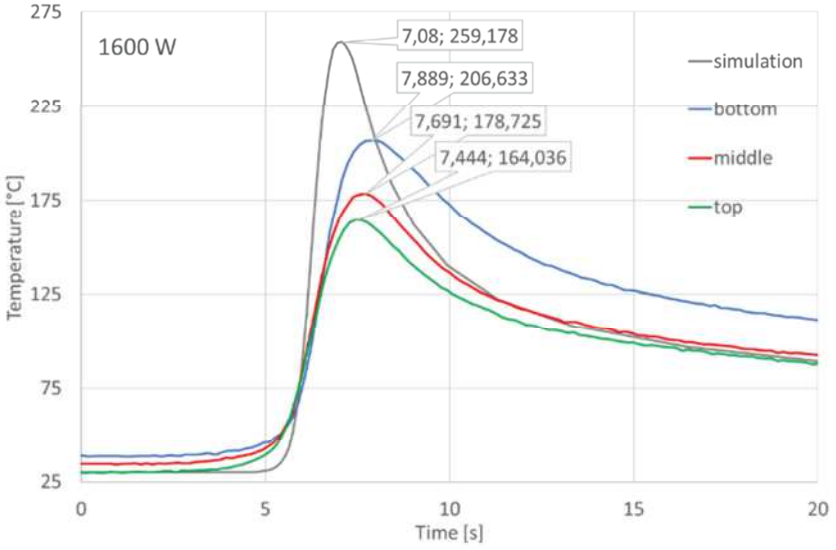


Fig. 6. Increasing error in temperature measurement on thermocouple no. 3

For this thermocouple increasing laser beam power, which with constant welding speed increases welding linear energy, the measured temperatures are increasingly lower compared to calculated values, Figure 6. This is the result of the inertial behaviour of the measuring method. This makes the heat cycle measured close to welding with this method high error rate. This is problematic as heat cycles nearest the path are most important when analysing welding and working out causes of reduced weldability. Incorrect placement of thermocouple in drilled channels results in an increasing difference between the ideal heat cycle and the measured one. The proposed resolution for reducing this difference is the change of measured temperature node placement to the actual placement of thermocouple. This would be possible after determining real thermocouple placement after destructive testing made post-heat cycle acquisition. This method can be used when measured data is used to scale, correct and verify simulation.

After recalculation of simulation with corrected plotted node placement, results were compared to measured results. Most accurate resulted from thermocouple condenser welded to the edge of the drilled hole. These results present very high convergence with simulation and surprisingly sharply reducing the inertia of thermocouple (the decreased difference between highest temperature and heating and cooling speeds. This could be caused by the increase of energy concentration and resistance during condenser welding of the thermocouple to sample resulting in the increased contact area. The sample results plots of the corrected model and measured values are shown in Figure 7.

The tests of laser hardening and remelting allowed for determining the basic geometric dimensions of the stitches, i.e. the width and depth of hardening/remelting, Table 4. A comparison of these values with the dimensions obtained in the case of numerical analyses allowed validation of the created numerical model. Comparison of the results of calculations with the results of real tests of laser hardening and remelting confirms the considerable compliance of the dimensions of the obtained stitches and their shape for both the case of hardening and remelting, Figures 8 and 9.

Also, temperature measurements made with thermocouples show high compliance of the recorded thermal cycles with those calculated for both hardening and laser remelting cases, Figures 10-12. For H1 bead – as indicated in Table 4, no hardening was obtained. The recorded and calculated thermal cycles confirm this situation because the maximum temperatures do not exceed the metallurgical transformation temperature, Figure 10. However it should be noted, that transformation temperatures are different and changed if very fast heating rates are used (in comparison with transformation temperatures used from CCT diagrams). These differences can be very small (about 20°C) for low carbon steels but also very big (even a 100°C) for high alloyed steels [25].

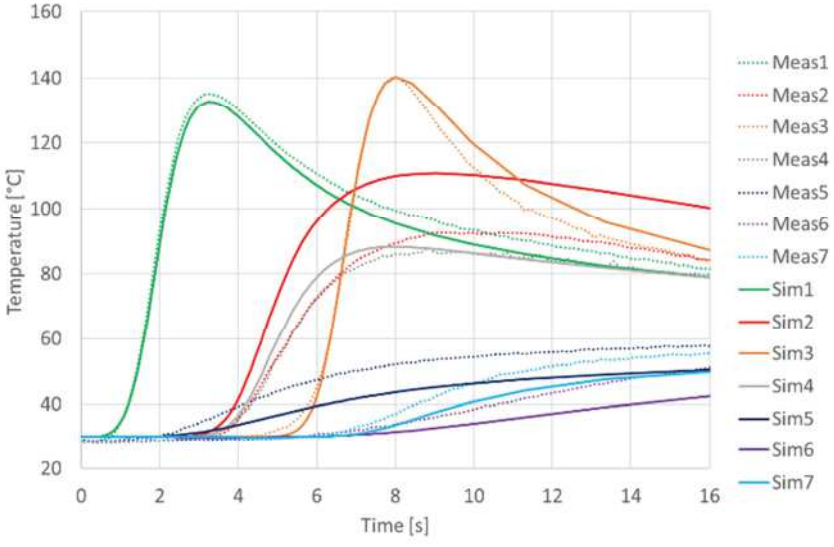


Fig. 7. Heat cycle from HPDL power 1200 W and top placement of thermocouples and corrected placement of nodes in the simulated model

Table 4.
Geometric dimensions of hardening and laser remelting beads

| Bead designation | Real bead width*, mm | Real bead depth*, mm | Calculated bead width, mm | Calculated bead depth, mm |
|---|---|---|---|---|
| Laser hardening | | | | |
| H1 | | | No hardening obtained | |
| H2 | 3.3 | 0.20 | 3.5 | 0.19 |
| H3 | 4.9 | 0.285 | 4.66 | 0.34 |
| H4 | 4.5 | 0.38 | 4.63 | 0.45 |
| H5 | 4.5 | 0.35 | 4.32 | 0.42 |
| H6 | 4.53 | 0.44 | 4.54 | 0.53 |
| H7 | 4.64 | 0.54 | 4.44 | 0.44 |
| H8 | 4.24 | 0.39 | 4.5 | 0.45 |
| H9 | 4.81 | 0.53 | 4.67 | 0.52 |
| H10 | 5.02 | 0.67 | 4.81 | 0.65 |
| Laser remelting | | | | |
| R1 | 4.15 | 0.30 | 4.10 | 0.35 |
| R2 | 4.46 | 0.32 | 4.51 | 0.54 |
| R3 | 4.80 | 0.41 | 4.48 | 0.93 |
| R4 | 5.48 | 0.50 | 5.13 | 0.45 |
| R5 | 5.65 | 0.63 | 5.36 | 0.71 |
| R6 | 5.18 | 0.48 | 4.81 | 0.46 |
| R7 | 4.45 | 0.36 | 4.63 | 0.42 |
| R8 | 4.48 | 0.36 | 3.92 | 0.33 |

* – in the case of the hardening process – the term bead should be understood as the area whose properties have changed

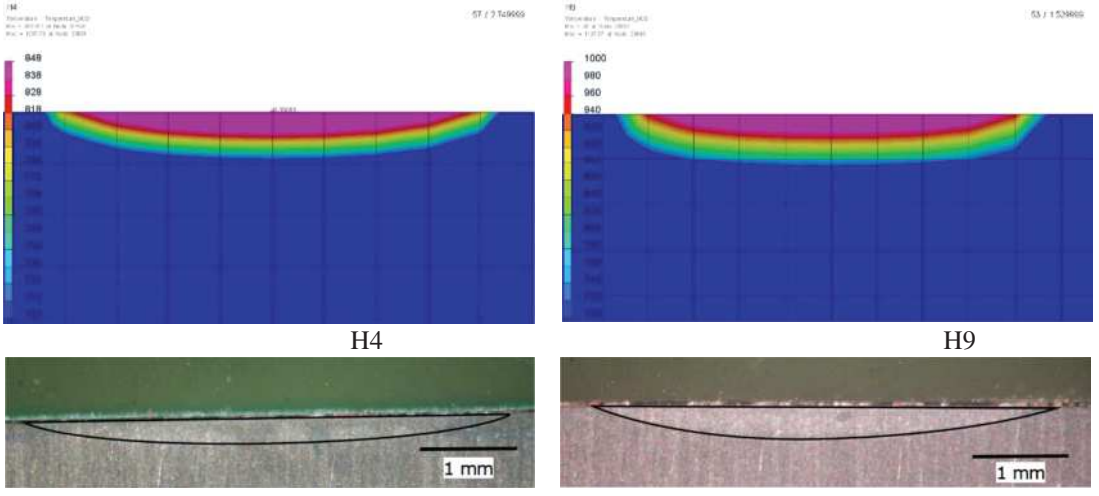


| Geometric dimensions of the bead | | |
|---|---|---|
| | Measured | Calculated |
| Bead width, mm | H4: 4.50<br>H9: 4.81 | H4: 4.63<br>H9: 4.67 |
| Bead depth, mm | H4: 0.38<br>H9: 0.53 | H4: 0.45<br>H9: 0.52 |

Fig. 8. Comparison of temperature distribution during WCL steel laser hardening with the image of the bead macrostructure

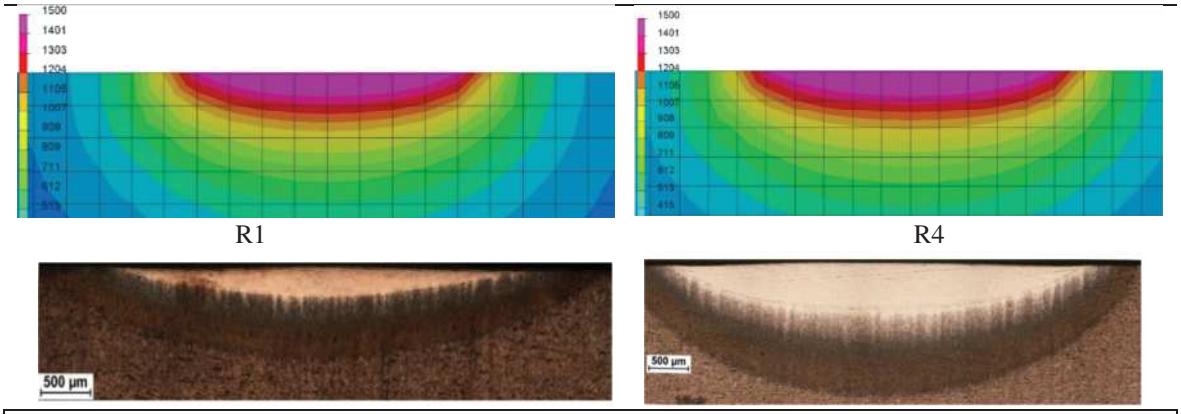


| Geometric dimensions of the bead | | |
|---|---|---|
| | Measured | Calculated |
| Bead width, mm | R1:4.15<br>R4: 5.48 | R1: 4.10<br>R4: 5.13 |
| Bead depth, mm | R1: 0.30<br>R4: 0.50 | R1: 0.35<br>R4: 0.45 |

Fig. 9. Comparison of temperature distribution during WCL steel laser remelting with the image of the bead macrostructure

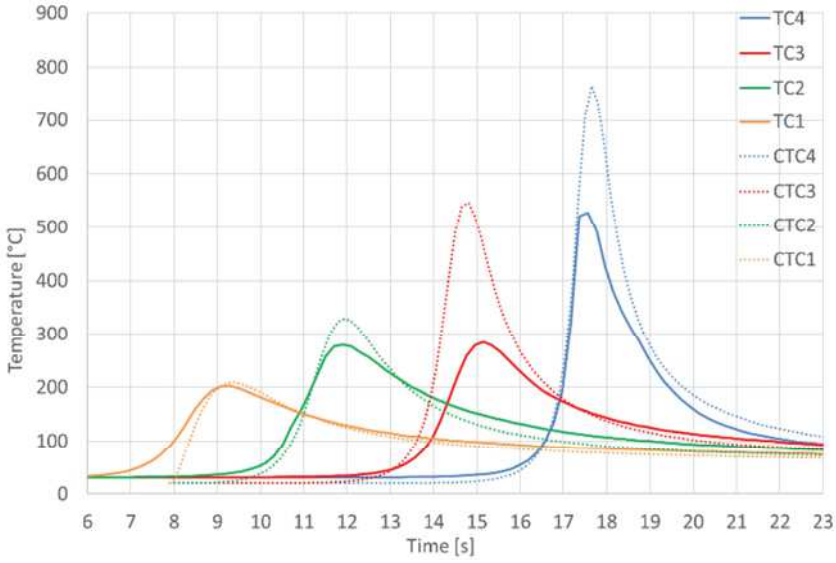


Fig. 10. Registered (TCx) and calculated (CTCx) thermal cycles at selected test locations of the H1 sample

In the case of presented laser hardening data, the difference in the maximum recorded value and calculated temperature value for TC3 and TC4 thermocouples is visible, where for the other two thermocouples these values are similar, Figure 11.

The reason for the differences, as it turned out after checking the position of the thermocouple welded in the hole made in the bottom of the sample, was the wrong location (place of welding) of the thermocouple. Correct heating of the element at the measurement site allowed to obtain a high convergence of the recorded and calculated results, Figure 12.

The recording of thermographic images with the half temperature distribution obtained as a result of the simulation also showed considerable similarities in the shape of the temperature field depending on the speed of heat source movement along a given trajectory, Figure 13.

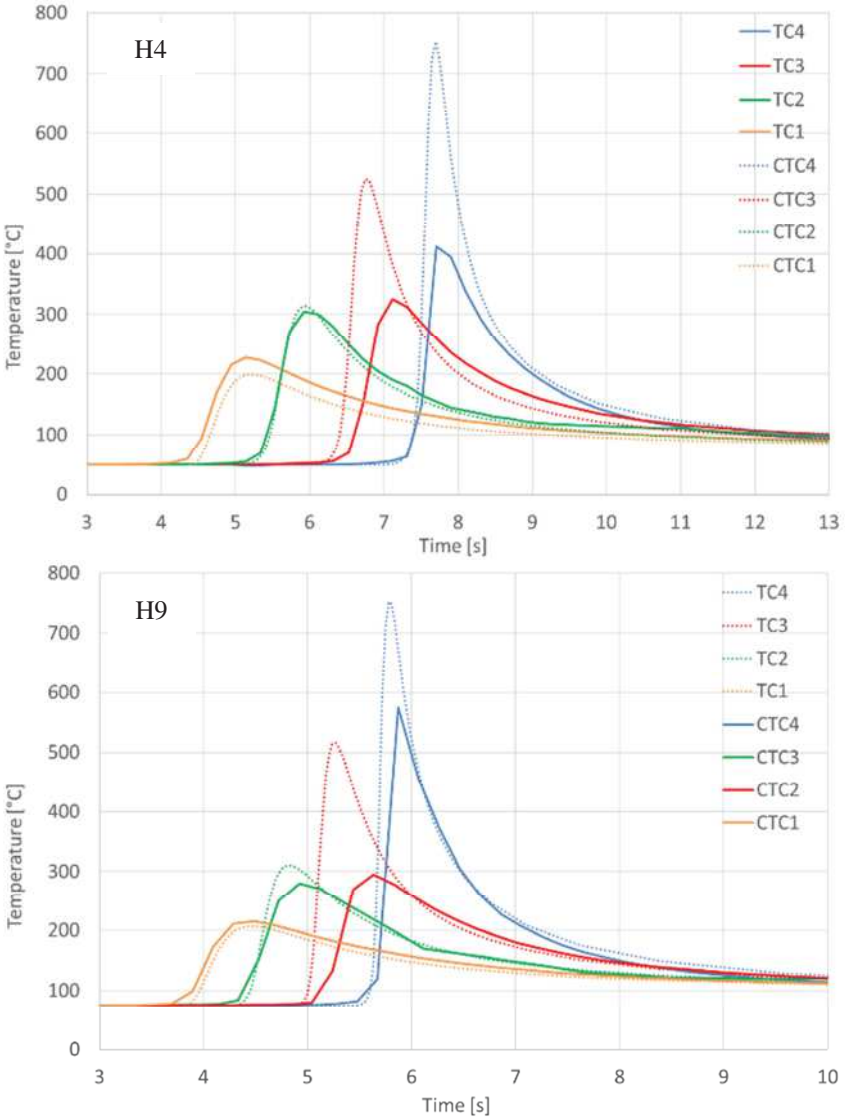


Fig. 11. Registered (TCx) and calculated (CTCx) thermal cycles in selected places of tested samples

However, thermographic measurements also showed disadvantages of this method of recording results in welding processes. The thermographic images show considerable noise caused probably by the heterogeneity of the emissivity factor. In the case of remelting the sample surface, it is necessary to determine the emission factors for melted and only heated areas, which significantly complicates both the process of processing the results and also their interpretation.

Table 5 shows the measured hardness HV1 for the WCL steel specimens. At this moment the calculation of the hardness is not completed because of WCL material database preparation for hardness calculations. The proposed model and methodology will be helpful in finishing the preparation of the hardness computation model for WCL steel.

## 5. Conclusions

The research on the process of laser hardening and remelting of WCL steel samples described in the article allowed observation of many factors affecting the measurement, but also the assessment of the process.

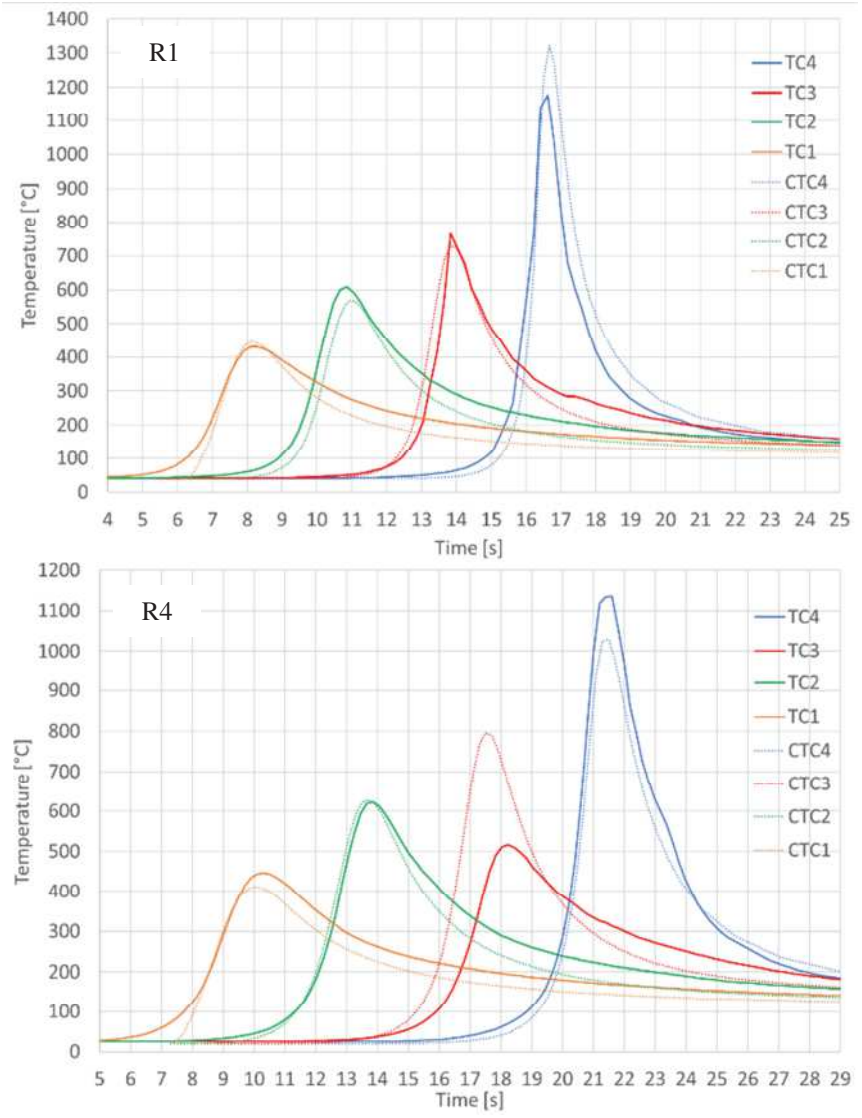


Fig. 12. Registered (TCx) and calculated (CTCx) thermal cycles in selected places of tested samples

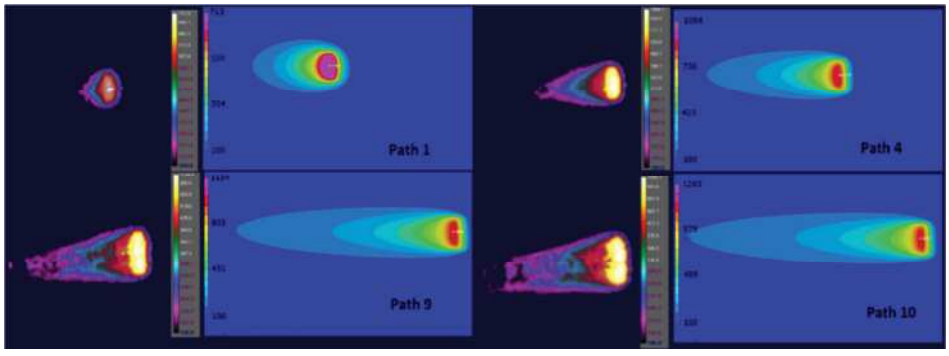


Fig. 13. Thermographic images (in the left columns) and calculated temperature field distributions (in the right columns) in the process of laser quenching – samples H1, H4, H9 and H10

Table 5.
Measured hardness HV1 after laser surface hardening or remelting of WCL steel specimens

| | H1 | H4 | H9 | R1 | R4 |
|---|---|---|---|---|---|
| Bead | - | - | - | 472<br>451<br>424 | 451<br>449<br>413 |
| Heat-affected zone | - | 600<br>546<br>378 | 280<br>250<br>229 | 360<br>344<br>349 | 258<br>298<br>274 |
| Base material | 204<br>206<br>218 | 204<br>203<br>210 | 210<br>207<br>209 | 205<br>207<br>209 | 209<br>207<br>208 |

The high consistency between the shape of the obtained temperature distributions and thermographic images compared with the results of actual tests, suggests that the differences in the maximum values of recorded and calculated thermal cycles can also be caused by temperature measurement errors. The presented study proves the high impact of faulty measuring element placement on measured heat cycles. This is a valid problem as non-destructive verification of measuring element placement is not possible when drilled hole placement is used. Another defined high error cause is inertial behaviour of measuring element, probably caused by to small contact patch between element and sample or too big diameter of the spherical thermocouple. Due to described problems, useful and free of these faults are well prepared numerical simulations. They give us the possibility to avoid some technical disturbances and offer very high repeatability in analyses, especially when we take into consideration lots of variants. As presented results shown, compared to the real measurement tests, FEM analyses offer also the high level of coherence between calculated and real values. This enables the use of collected data for scaling, correction and verification of simulation when faulty placement of measuring element is detected after measurements were taken in lieu of retaking measurements which can be costly and time-consuming.

As it was mentioned, the reason for these discrepancies should be sought here in the very construction of the measurement. Both the method of attaching the spherical thermocouple tip and the limited, with a multi-channel measurement, the sampling frequency causes errors in the measurement of the maximum temperature (since the slope of the cooling curve is in most cases compatible). Also, measurements made using a thermal imaging camera showed that there are significant problems with recording thermograms, especially if the sample material on the surface is melted.

Analysis of the results of the experiments shows that, in the case of the laser hardening process, no correlation was observed between the linear energy and the shape and dimensions of the hardened zone, which is confirmed in practice, where multiple attempts and extensive experience in conducting the process are needed to optimize the laser hardening technology. In the case of the laser remelting process, this relationship is more clearly visible, where the dimensions of the obtained bead increase with the increase of the linear energy of the process.

To sum up, in light of the presented problems, numerical simulations are an interesting alternative in the development of laser hardening and remelting technology. After proper calibration and validation of the numerical model, they allow for predicting the volumetric distribution of temperature fields with high accuracy as well as the geometrical dimensions of the beads obtained, which, combined with the engineering knowledge of the staff, allows for efficient and precise optimization of the technological process.

## References

[1] J. Dosset, G.E. Totten, ASM Handbook Volume 4A: Steel Heat Treating Fundamentals and Processes, ASM International, 2013.

[2] A. Lisiecki, Study of Optical properties of surface layers produced by laser surface melting and laser surface nitriding of titanium alloy, Materials 12 (2019) 3112, DOI: https://doi.org/10.3390/ma12193112.

[3] D. Janicki, Microstructure and sliding wear behaviour of in-situ TiC-reinforced composite surface layers fabricated on ductile cast iron by laser alloying, Materials 11/1 (2018) 75, DOI: https://doi.org/10.3390/ma11010075.

[4] G. Moskal, A. Grabowski, A. Lisiecki, Laser remelting of silicide coatings on Mo and TZM alloy, Solid State Phenomena 226 (2015) 121-126, DOI: https://doi.org/10.4028/www.scientific.net/SSP.226.121.

[5] B.S. Yilbas, F. Patel, C. Karatas, Laser controlled melting of H12 hot-work tool steel with $B_4C$ particles at the surface, Optics & Laser Technology 74 (2015) 36-42, DOI: https://doi.org/10.1016/j.optlastec.2015.05.012.

[6] A. Klimpel, L.A. Dobrzański, A. Lisiecki, D. Janicki, The study of properties of Ni-WC wires surfaced deposits, Journal of Materials Processing Technology 164-165 (2005) 1046-1055, DOI: https://doi.org/10.1016/j.jmatprotec.2005.02.195.

[7] M. Tobar, C. Alvarez, J. Amado, A. Ramil, E. Saavedra, A Yanez, Laser transformation hardening of a tool steel: Simulation-based parameter optimization and experimental results, Surface and Coatings Technology 200/22-23 (2006) 6362-6367, DOI: https://doi.org/10.1016/j.surfcoat.2005.11.067.

[8] D. Janicki, Fabrication of high chromium white iron surface layers on ductile cast iron substrate by laser surface alloying, Strojniski Vestnik 63 (2017) 705-714, DOI: https://doi.org/10.5545/sv-jme.2017.4379.

[9] J. Górka, D. Janicki, M. Fidali, W. Jamrozik, Thermographic Assessment of the HAZ Properties and Structure of Thermomechanically Treated Steel, International Journal of Thermophysics 38/12 (2017) Article number 183, DOI: https://doi.org/10.1007/s10765-017-2320-9.

[10] A. Lisiecki, Mechanisms of hardness increase for composite surface layers during laser gas nitriding of the Ti6Al4V alloy, Materiali in Tehnologije 51/4 (2017) 577-583, DOI: https://doi.org/10.17222/mit.2016.106.

[11] A. Lisiecki, Mechanism of laser surface modification of the Ti-6Al-4V alloy in nitrogen atmosphere using a high power diode laser, Advanced Materials Research 1036 (2014) 411-416, DOI: https://doi.org/10.4028/www.scientific.net/AMR.1036.411.

[12] T. Chmielewski, D. Golański, The role of welding in the remanufacturing process, Welding International 29/11 (2015) 861-864, DOI: https://doi.org/10.1080/09507116.2014.937604.

[13] A. Lisiecki, D. Ślizak, A. Kukofka, Robotic fiber laser cladding of steel substrate with iron-based metallic powder, Materials Performance and Characterization 8/6 (2019) 1202-1213, DOI: https://doi.org/10.1520/MPC20190068.

[14] B. Wyględacz, T. Kik, D. Janicki, Numerical simulation and heat cycle examination of WCL steel laser hardening, Welding Technology Review 89/5 (2017) 91-95 DOI: https://doi.org/10.26628/wtr.v89i5.773 (in Polish).

[15] T. Kik, M. Burda, Numerical simulation in laboratory research of welding processes as a tool for study CNT stability in molten metal, Proceedings of the First International Conference on Modern Manufacturing Technologies in Industrial Engineering "ModTech 2013", Sinaia, Romania, 2013; in: C. Carausu (Ed.), Book of abstracts, Modtech Publishing House, Iasi, 2013, 18.

[16] L. Salbut, M. Kujawinska, M. Jozwik, D. Golanski, Investigation of ceramic-to-metal joint properties by hybrid moire interferometry/FEM analysis, Proceedings of SPIE 3745 (1999) 298-306, DOI: https://doi.org/10.1117/12.357791.

[17] C.S. Pathak, L.G. Navale, A.D. Sahasrabudhe, M.J. Rathod, Analysis of Thermal Cycle during Multipass Arc Welding, Welding Journal 91/5 (2012) 149-154.

[18] Welding simulation user guide 2016, SYSWELD manual, ESI Group.

[19] J. Bradáč, Calibration of heat source model in numerical simulations of fusion welding, Machines, Technologies, Materials 11 (2013) 9-12.

[20] A. Sajek, Application of FEM simulation method in area of the dynamics of cooling AHSS steel with a complex hybrid welding process, Welding in the World 63/4 (2019) 1065-1073, DOI: https://doi.org/10.1007/s40194-019-00718-z.

[21] W. Wu, N. Liang, C. Gan, G. Yu, Numerical investigation on laser transformation hardening with different temporal pulse shapes, Surface and Coatings Technology 200/8 (2006) 2686-2694, DOI: https://doi.org/10.1016/j.surfcoat.2004.11.011.

[22] M. Vanek, J. Moravec, J. Rihacek, Improvement of Model of Aluminium Alloys Behaviour for Application in Numerical Simulations of Welding, Modern Machinery (MM) Science Journal November (2016) 1370-1375, DOI: https://doi.org/10.17973/MMSJ.2016_11_2016124.

[23] J. Moravec, M. Slováček, Application of Numerical Simulations at Welding Multilayer Welds from the Material X22CrMoV12-2, Advanced Materials Research 1029 (2014) 31-36, DOI: https://doi.org/10.4028/www.scientific.net/AMR.1029.31.

[24] J. Moravec, J. Bradáč, I. Nováková, Ways of Numerical Prediction of Austenitic Grain Size in Heat-Affected Zone of Welds, Advanced Materials

Research 1029 (2014) 25-30, DOI: https://doi.org/10.4028/www.scientific.net/AMR.1029.25.

[25] J. Moravec, M. Dikovits, I. Novakova, O. Caliskanoglu, A comparison of dilatometry results obtained by two different devices when generating CCT and in-situ diagrams, Key Engineering Materials 669 (2016) 477-484, DOI: https://doi.org/10.4028/www.scientific.net/KEM.669.477.